Since January 2020 Elsevier has created a COVID-19 resource centre with free information in English and Mandarin on the novel coronavirus COVID-19. The COVID-19 resource centre is hosted on Elsevier Connect, the company's public news and information website.

Available online at www.sciencedirect.com
SCIENCE DIRECT®
Virus Research 107 (2005) 141–149
Virus Research
www.elsevier.com/locate/virusres

Incorporation fidelity of the viral RNA-dependent RNA polymerase: a kinetic, thermodynamic and structural perspective☆

Christian Castro, Jamie J. Arnold, Craig E. Cameron*

Department of Biochemistry and Molecular Biology, Pennsylvania State University, University Park, PA 16802, USA

Available online 8 December 2004

Abstract

Positive-strand RNA viruses exist as a quasi-species due to the incorporation of mutations into the viral genome during replication by the virus-encoded RNA-dependent RNA polymerase (RdRP). Therefore, the RdRP is often described as a low-fidelity enzyme. However, until recently, a complete description of the kinetic, thermodynamic and structural basis for the nucleotide incorporation fidelity of the RdRP has not been available. In this article, we review the following: (i) the steps employed by the RdRP to incorporate a correct nucleotide; (ii) the steps that are employed by the RdRP for nucleotide selection; (iii) the structure-based hypothesis for nucleotide selection; (iv) the impact of sites remote from the active site on polymerase fidelity. Given the recent observation that RNA viruses exist on the threshold of error catastrophe, the studies reviewed herein suggest novel strategies to perturb RdRP fidelity that may lead ultimately to the development of antiviral agents to treat RNA virus infection.

Keywords: Polymerase fidelity; RdRP; Nucleotide selection

1. Introduction

Positive-strand RNA viruses cause a number of human diseases, including the common cold, myocarditis, hepatitis and severe acute respiratory syndrome (SARS). Treatment of RNA virus infection has proven to be a challenging task. However, even if effective therapeutics existed, the quasi-species nature of RNA viruses would facilitate the emergence of virus variants that are resistant to antiviral therapy.

The variability displayed in RNA virus populations can be attributed to mutations introduced into the genome by the viral replicase during each round of replication. The viral replication machinery is a complex assembly of viral, and in some cases, host proteins. However, at the heart of the replication machinery is the virus-encoded RNA-dependent RNA polymerase (RdRP). RdRPs have been shown to display a high mutation rate compared to their DNA counterparts (Drake, 1993, 1999). This decrease in fidelity exhibited by RdRPs has been suggested to be the primary contributing factor for the variability in RNA virus genomes.

Numerous studies have documented the high mutation frequency exhibited by RNA viruses as well as their rapid rates of evolution (De la Torre et al., 1990; Domingo, 1989; Domingo et al., 1985, 1996; Drake, 1993, 1999; Drake and Holland, 1999; Holland et al., 1982, 1990). The determination of RNA virus mutation frequencies has been accomplished by evaluating the following: (i) development of resistance to antiviral agents; (ii) escape from monoclonal antibody treatment; (iii) changes in virus fitness; (iv) serial passage of the virus in cell culture or in vivo followed by direct sequencing (Table 1). Unfortunately, mutations that produce replication-incompetent or perhaps translation-incompetent genomes are not scored in these assays. Therefore, direct measurements of the intrinsic error rate of the RdRP obtained from in vitro analysis is the simplest approach to define the upper limit for the mutational frequency of a RNA virus.

The genetic variability of RNA viruses is advantageous and allows viruses to adapt to environmental changes more

☆ This work was supported, in part, by a grant (AI45818) from the NIAID, National Institutes of Health. C.E.C. is the recipient of an established investigator award (0340028N) from the American Heart Association.
* Corresponding author. Tel.: +1 814 863 8705; fax: +1 814 865 7927.
E-mail address: cec9@psu.edu (C.E. Cameron).

0168-1702/$ – see front matter © 2004 Elsevier B.V. All rights reserved.
doi:10.1016/j.virusres.2004.11.004

Table 1
Mutation frequencies[a] of selected RNA viruses

Virus	Mutation frequency	Assay	References
PV-1	5.4×10^{-3}–7×10^{-4}	Biochemical assay[b]	Ward et al. (1988)
PV-1	2.1×10^{-4}	GuaD–GuaR[c]	De la Torre et al. (1990)
PV-1	7.8×10^{-5}–4×10^{-8}	GuaD–GuaR	Pincus et al. (1986)
Coxsackie A9	1×10^{-4}	2-HBB resistance[d]	Eggers and Tamm (1965)
Influenza A	1.5×10^{-5}	Plaque assay[e]	Parvin et al. (1986)
VSV	1×10^{-3}–1×510^{-4}	Plaque assay	Steinhauer et al. (1989)
PV-1	2.1×10^{-4}	Sequencing[f]	Crotty et al. (2001)
HAV	1×10^{-3}–1×10^{-4}	Sequencing	Sanchez et al. (2003)
TMV	3×10^{-4}	Sequencing	Kearney et al. (1999)
HCV	$\sim 1 \times 10^{-3}$	Sequencing	Young et al. (2003)
FMDV	1.4×10^{-4}	Sequencing	Airaksinen et al. (2003)
HTNV	1.1×10^{-3}	Sequencing	Severson et al. (2003)
LCMV	3.6×10^{-4}	Sequencing	Ruiz-Jarabo et al. (2003)

[a] Mutation frequency is defined as the number of mutations per replication event.
[b] Amount of a noncomplementary nucleotide incorporated divided by the total amount of complementary and noncomplementary nucleotide incorporated using homopolymeric RNA templates.
[c] Reversion of guanidine dependant to guanidine resistant.
[d] Development of resistance to 2-(α-hydroxybenzyl)-benzimidazole (2-HBB).
[e] Mutations were determined by sequencing different plaques developed after infection with a single clone.
[f] Viral population samples from the host organism or cell culture were isolated, amplified and sequenced.

rapidly; however, a consequence of this same genetic variability is the enhanced sensitivity of the viral population to accumulation of additional mutations (Holland et al., 1990; Irurzun et al., 1992; Lee et al., 1997). As the number of mutations in the viral genomes increases and passes this error threshold, the fitness decreases significantly, ultimately resulting in extinction. Therefore, agents that increase the mutation frequency of the virus should be effective antivirals. This prediction was confirmed by studies of ribavirin that showed that the mechanism of action of this antiviral agent is lethal mutagenesis (Crotty et al., 2001, 2000).

Given the importance of incorporation fidelity for the viability of RNA viruses and the potential to exploit small-molecule modulators of incorporation fidelity as antiviral agents, a precise description of the molecular basis for incorporation is warranted. In this article, we review the kinetic and thermodynamic analysis of correct and incorrect nucleotide incorporation catalyzed by the RdRP from poliovirus ($3D^{pol}$) highlighting the steps that are essential for nucleotide substrate selection. In addition, we review the structure-based hypothesis for $3D^{pol}$ fidelity that likely extends to all animal virus RdRPs.

2. Kinetic mechanism of nucleotide incorporation for poliovirus $3D^{pol}$

In order to establish a system to preclude heterogeneous binding of $3D^{pol}$ to primer/template, thereby permitting mechanistic analysis, a novel substrate was designed (Fig. 1) (Arnold and Cameron, 2000). This RNA substrate consists of a 10-nucleotide heteropolymeric RNA that is self-complementary and forms a six base-pair duplex region with an identical 4-nucleotide 5′-overhang on both sides of

Fig. 1. Symmetrical primer template substrate (sym/sub) used to study poliovirus polymerase $3D^{pol}$-catalyzed nucleotide incorporation.

the primer/template. Both 3′-hydroxyls of the substrate are competent for templated extension resulting in a symmetrical substrate, termed sym/sub (Arnold and Cameron, 2000) (Fig. 1). The enzyme binds productively to sym/sub regardless of the orientation of binding and regardless of which of the two 3′-hydroxyls is in the catalytic center. The 4-nucleotide template permits either single or multiple rounds of nucleotide incorporation to be evaluated by selecting the appropriate nucleotide or nucleotides employed in the reaction. $3D^{pol}$–sym/sub complexes recapitulate a biologically relevant elongation complex (Gohara et al., 2000); therefore, analysis of the mechanism of nucleotide incorporation in vitro using this substrate is likely to be relevant to the reaction in vivo.

Evaluation of the kinetics of nucleotide incorporation into sym/sub by $3D^{pol}$ has revealed information on the binding of the incoming nucleotide, the maximal rate of nucleotide incorporation and the specificity of nucleotide incorporation (Table 2). These parameters are expressed by the kinetic constants: $K_{d,app}$, k_{pol} and $k_{pol}/K_{d,app}$, respectively (Arnold and Cameron, 2004b). The fidelity of the viral RdRP can be obtained by comparing $k_{pol}/K_{d,app}$ values for correct and incorrect nucleotides. A complete kinetic and thermodynamic analysis of poliovirus $3D^{pol}$-catalyzed nucleotide incorporation revealed that nucleotide incorporation can be described by the five steps shown in Scheme 1 (Arnold and Cameron, 2004b). The $3D^{pol}$–sym/sub complex (ER_n) binds nucleotide (NTP) to form a ternary complex (ER_nNTP) that under-

Table 2
Kinetic parameters for 3D^{pol}-catalyzed nucleotide incorporation

Substrates		Kinetic parameters			Fidelity[a]
Nucleic acid	Nucleotide	$K_{d,app}$ (μM)	k_{pol} (s^{-1})	k_{pol}/K_d ($\mu M^{-1} s^{-1}$)	
sym/sub-U					
GCA**U**GGGCCC	ATP	134 ± 18	87 ± 4	0.65	–
CCCGGG**U**ACG	2′-dATP	284 ± 59	0.80 ± 0.06	2.8×10^{-3}	230
	3′-dATP	317 ± 51	1.4 ± 0.1	4.4×10^{-3}	150
	CTP	>500 μM	<0.0025 s^{-1}	$<5 \times 10^{-6}$	$>2.0 \times 10^{5}$
	GTP	430 ± 98	0.014 ± 0.003	3.3×10^{-5}	2.3×10^{4}
	UTP	>500 μM	<0.0025 s^{-1}	$<5 \times 10^{-6}$	$>2.0 \times 10^{5}$

[a] Fidelity is calculated as $[(k_{pol}/K_{d,app})_{ATP} + (k_{pol}/K_{d,app})_{incorrect}]/[(k_{pol}/K_{d,app})_{incorrect}]$ (Patel et al., 1991), reproduced with permission from Biochemistry.

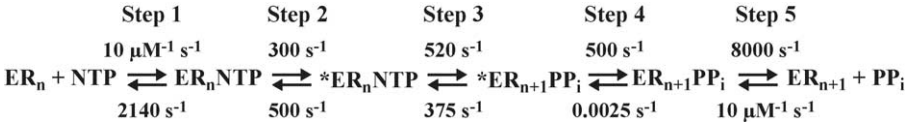

Scheme 1. Complete kinetic mechanism for 3D^{pol}-catalyzed nucleotide incorporation.

goes a conformational change to form a complex that is competent for phosphoryl transfer ($^{*}ER_nNTP$). Chemistry occurs, forming a ternary product complex ($^{*}ER_{n+1}PP_i$); this complex isomerizes to form a ternary product complex ($ER_{n+1}PP_i$) from which PP_i can dissociate. After dissociation of PP_i, a 3D^{pol}–sym/sub product complex (ER_{n+1}) remains that is competent for the next cycle of nucleotide incorporation. For poliovirus 3D^{pol}, two steps in the mechanism are partially rate-limiting for correct nucleotide incorporation: the conformational-change step (step 2) prior to phosphoryl transfer and the phosphoryl-transfer step (step 3) (Arnold and Cameron, 2004b).

The kinetic and thermodynamic analysis of correct nucleotide incorporation described above has been interpreted by using the structural model for the 3D^{pol}–sym/sub–ATP complex illustrated in Fig. 2. Binding of the incoming nucleotide in complex with divalent cation to the 3D^{pol}–primer/template complex is driven by the metal-complexed triphosphate moiety of the nucleotide (Fig. 2A). Once bound, a conformational change occurs to bring the metal-complexed triphosphate moiety into the appropriate position to interact with the conserved aspartyl groups of the enzyme, and at the same time, organizes the active site for acceptance of the second metal ion required for catalysis (Fig. 2B). Finally, catalysis occurs (Fig. 2C).

3. Kinetic basis for fidelity of nucleotide incorporation

It has been well documented that substitution of Mn^{2+} for Mg^{2+} as the divalent cation cofactor in polymerase-catalyzed reactions decreases the stringency of substrate selection and incorporation fidelity (Arnold et al., 1999; Beckman et al., 1985; Goodman et al., 1983; Huang et al., 1997; Liu and Tsai, 2001; Tabor and Richardson, 1989). However, the detailed mechanistic basis for the destructive effects of Mn^{2+} was not completely understood until recently (Arnold et al., 2004). By using Mn^{2+} as the divalent cation cofactor, the ability to diminish the rate of phosphoryl transfer for incorrect nucleotides relative to correct nucleotides is lost completely, leaving only the conformational-change step for nucleotide selection (Scheme 2) (Arnold et al., 2004). When Mn^{2+} is employed as the divalent cation, the conformation of

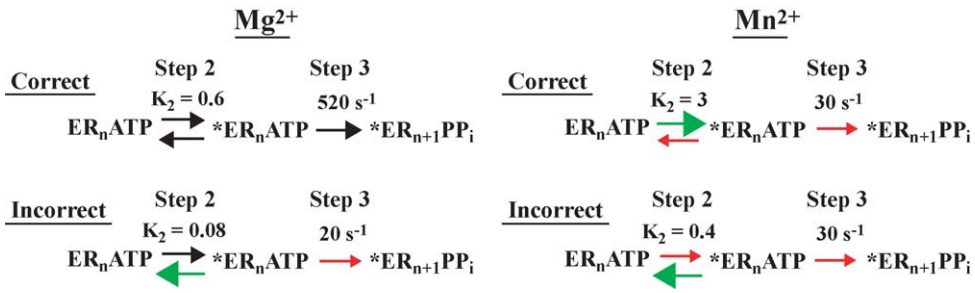

Scheme 2. Comparison of the conformational-change step and the phosphoryl-transfer step for 3D^{pol}-catalyzed correct and incorrect nucleotide incorporation in the presence of Mg^{2+} and Mn^{2+}.

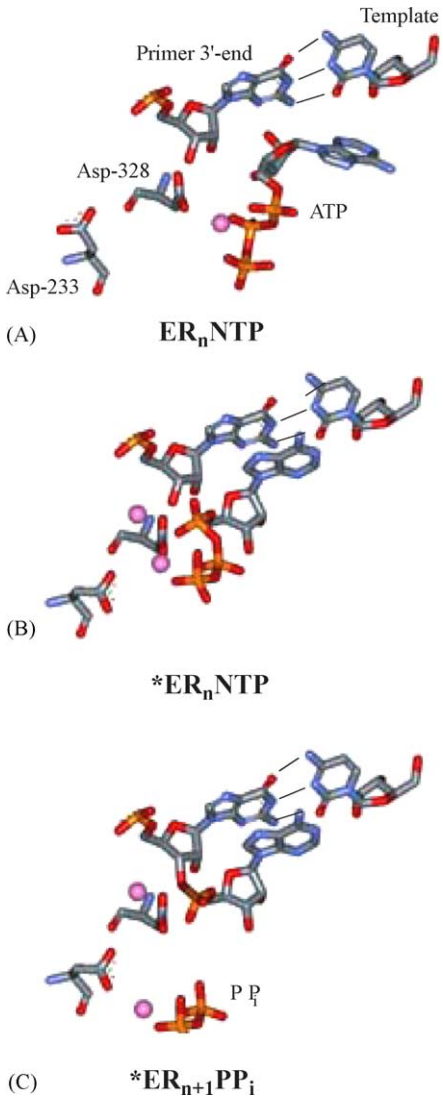

Fig. 2. Structural model for 3D^{pol}-catalyzed nucleotide incorporation: (A) ground-state binding of metal-complexed nucleotide; (B) reorientation of the triphosphate into the catalytically competent configuration; (C) phosphoryl transfer and pyrophosphate release. While the kinetic mechanism suggests a conformational change prior to pyrophosphate release, kinetic data do not provide any information to permit a molecular description of this step. Images were generated from the model previously described (Gohara et al., 2000). Nucleotide and side chain motions were derived from (Johnson et al., 2003) by approximate rotation and translation movements. Atom colors correspond to the following: red, oxygen; blue, nitrogen; gray, carbon; magenta, Mg^{2+} or Mn^{2+}. The images were rendered with WebLab Viewer Pro (Accelrys Inc., San Diego, CA). Reproduced with permission from Biochemistry (2004), submitted. © 1998 Am. Chem. Soc.

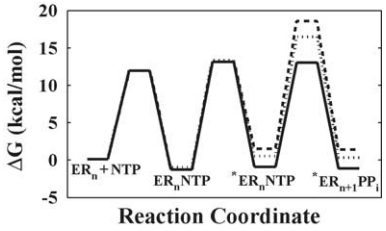

Fig. 3. Comparison of the free energy profile for correct and incorrect 3D^{pol}-catalyzed nucleotide incorporation in the presence of Mg^{2+}. The free energy profile for correct and incorrect nucleotide incorporation are shown as follows: solid line for AMP incorporation, small dotted line for 2′-dAMP incorporation, and large dotted line for GMP incorporation. The concentrations of the substrates and products used were 2000 μM NTP and 20 μM PP_i. The free energy for each reaction step was calculated from $\Delta G = RT[\ln(kT/h) - \ln(k_{obs,for})]$, where $R = 1.99$ cal K^{-1} mol^{-1}, $T = 303$ K, $k = 3.30 \times 10^{-24}$ cal K^{-1}, $h = 1.58 \times 10^{-34}$ cal s and k_{obs} is the first-order rate constant (Arnold et al., 2004). The free energy for each species was calculated from $\Delta G = RT[\ln(kT/h) - \ln(k_{obs,for})] - RT[\ln(kT/h) - \ln(k_{obs,rev})]$. Reproduced with permission from Biochemistry, 2004, submitted. © 1998 Am. Chem. Soc.

the metal-bound triphosphate coupled with the additional adventitious interactions that can occur between the enzyme and Mn^{2+} increases the stability of the activated ternary complex (Scheme 2, step 2). Compared to reactions in the presence of Mg^{2+}, the increase in stability of the activated ternary complex is the same regardless of the nature of the nucleotide (correct or incorrect). In addition, the capacity of Mn^{2+} to bind more tightly to the β and γ phosphates makes the orientation of the triphosphate independent of interactions with residues in the ribose-binding pocket. Consequently, perturbations in the orientation of the triphosphate will not occur in response to binding of a nucleotide with an incorrect base or sugar configuration. Therefore, the inability to couple the nature of the bound nucleotide to the efficiency of phosphoryl transfer is the primary reason for the observed loss of 3D^{pol} fidelity in the presence of Mn^{2+}.

Given that the conformational-change step (step 2) and the phosphoryl-transfer step (step 3) are partially rate-limiting for correct nucleotide incorporation, it was likely that these two steps were used to maximize polymerase fidelity. Restated, these two steps would be used by the enzyme to distinguish a correct nucleotide from an incorrect nucleotide. Through evaluation of the differences between correct and incorrect nucleotide incorporation catalyzed by 3D^{pol}, it was found that there is no difference in ground-state binding (step 1) regardless of the nucleotide substrate employed (Table 2, Fig. 3). Therefore, ground-state binding cannot contribute to the process of nucleotide substrate selection. The reason for this observation likely reflects the use of the triphosphate for ground-state binding instead of the ribose or base. However, the two steps in the kinetic mechanism for nucleotide incorporation catalyzed by 3D^{pol} that provide the greatest contribution to fidelity are formation of the activated ternary complex (step 2) and phosphoryl transfer (step 3) (Schemes 1 and 2, Fig. 3).

The conformational change preceding catalysis is thought to be reorientation of the metal-complexed triphosphate moiety of the nucleotide from its ground-state configuration (Fig. 2A) to the catalytically competent configuration (Fig. 2B) (Arnold et al., 2004). The greatest number of favorable interactions will occur with the correct nucleotide, permitting this step to provide some discrimination between correct nucleotides and nucleotides containing an incorrect

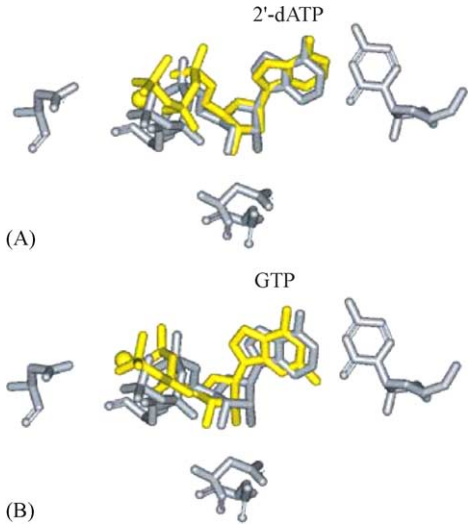

Fig. 4. Structural model for 3D^{pol}-catalyzed nucleotide incorporation fidelity. Yellow molecules indicate important structural changes: (A) possible conformation of 2′-dATP bound to the NTP-binding pocket; the change here could be caused by the different sugar pucker. (B) Possible conformation of GTP bound to the NTP-binding pocket; the change here could be caused by the non-planar G:U basepair. Reproduced with permission from Biochemistry, 2004, submitted. © 1998 Am. Chem. Soc.

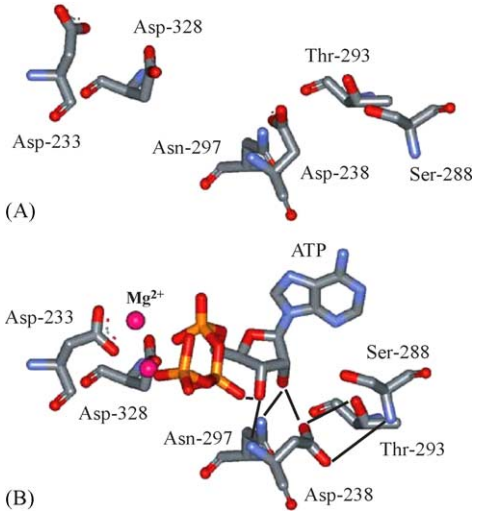

Fig. 5. Nucleotide-binding pocket of 3D^{pol}: (A) residues located in the NTP-binding pocket as observed in the unliganded structure of 3D^{pol} (Hansen et al., 1997); Asp-233 and Asp-238 are from structural motif A; Ser-288, Thr-293, and Asn-297 are from motif B; Asp-328 is from motif C. (B) Model for interaction of 3D^{pol} with bound nucleotide (Gohara et al., 2004); ATP and metal ions required for catalysis are labeled. In this model, the side chains for Asp-233 and Asp-238 have been rotated to permit interactions with ATP. Asp-238, Ser-288 and Thr-293 have been positioned to interact. The image was created by using the program WebLab Viewer (Molecular Simulations Inc., San Diego, CA). Reproduced with permission from Biochemistry, 2004, submitted. © 1998 Am. Chem. Soc.

base or sugar configuration. The presence of an incorrect sugar or base in the nucleotide-binding pocket can modify the nature and/or strength of the interactions with the actively oriented triphosphate causing a suboptimal organization of the complex for catalysis (Fig. 4).

In addition to the significant destabilization of the activated ternary complex, changes in the phosphoryl-transfer step occur when incorrect nucleotide substrates are utilized (Scheme 2, step 3). The decreased rate of chemistry for incorrect nucleotides is caused by the inability to maintain the triphosphate in the catalytically competent conformation and to maintain the appropriate distance between the α-phosphate and the 3′-OH (Scheme 2, step 3; Fig. 4).

4. Structural basis for fidelity

Sequence alignments of animal virus RdRPs have indicated the presence of several absolutely conserved amino acid residues that can be mapped to the nucleotide-binding pocket (Gohara et al., 2000, 2004; Hansen et al., 1997; Koonin, 1991). Six of these interact with the nucleotide substrate: Asp-233, Asp-238, Asp-328, Ser-288, Thr-293, and Asn-297 (Fig. 5A). In order to determine the importance of these residues for nucleotide selection, 3D^{pol} derivatives were created in which some of these residues were changed to alanine. The derivatives were subsequently purified and the mechanism of nucleotide selection determined by evaluating the kinetics of incorporation of correct and incorrect nucleotides (Gohara et al., 2000, 2004).

The results obtained from the studies of incorporation of correct and incorrect nucleotides with wild-type 3D^{pol} and the 3D^{pol} derivatives permitted the identification of essential amino acid residues and the interactions that are important for correct nucleotide selection. The model for nucleotide binding in Figs. 2 and 4 can be expanded to include these interactions. The first step is binding of the nucleotide in the ground state. In this ground-state configuration, the ribose cannot bind in a productive orientation because the interaction between Asp-238 and Asn-297 observed in the unliganded enzyme occludes the ribose-binding pocket (Gohara et al., 2000, 2004). A conformational change occurs that orients the triphosphate for phosphoryl transfer. This transition is proposed to be partially rate-limiting for correct nucleotide incorporation (step 2 in Scheme 1) (Arnold and Cameron, 2004b; Arnold et al., 2004). Moreover, the stability of the complex in this conformation will dictate the efficiency of phosphoryl transfer as any movement in the position of the triphosphate will produce either a suboptimal orientation or a suboptimal distance for catalysis. In order to maintain the triphosphate in the appropriate orientation, an extensive hydrogen-bonding network is involved that can be traced to residues in the ribose-binding pocket (Fig. 5B) (Gohara et al., 2004). Formation of this network requires reorientation of Asp-238 and Asn-297 as well as interaction of the oxygen of the β-phosphate with the 3′-OH of the nucleotide substrate. The position of the ribose is held firmly by interactions between the 3′-OH and the backbone of Asp-238 and

by interactions between the 2′-OH and Asn-297. The backbone of Asp-238 is restricted by the interaction of the Asp-238 side chain with other residues in the pocket, perhaps Ser-288 and Thr-293 (Fig. 5B). The appropriate organization of this complex will permit binding and/or alignment of the second divalent cation cofactor, permitting phosphoryl transfer, translocation and pyrophosphate release (Arnold and Cameron, 2004b; Arnold et al., 2004).

Reduced stabilization of the ribose moiety of the bound nucleotide caused by deleting interactions with the 2′-OH (e.g. 2′-dATP or N297A) may also alter the interaction between the 3′-OH and the β-phosphate of the nucleotide substrate, resulting in movement of the triphosphate and the consequent reduction in the efficiency of nucleotide incorporation. This model explains the observation that both the conformational change preceding phosphoryl transfer and phosphoryl transfer are reduced for 2′-dAMP incorporation by $3D^{pol}$ (Table 2) (Arnold and Cameron, 2004b; Arnold et al., 2004) or AMP incorporation by the N297A derivative (Gohara et al., 2000, 2004). Selection against nucleotides with other ribose modifications could employ a similar mechanism. These data are consistent with the conclusion that information on the nature of the interactions in the ribose-binding pocket can be disseminated to the catalytic center by using the conformation of the Asp-238 and the corresponding orientation of the triphosphate.

Possible perturbations of the triphosphate caused by binding of a nucleotide with an incorrect sugar or base are illustrated in Fig. 4A and B, respectively. In the G:U mispair, (GMP incorporation into sym/sub-U) the orientation of the triphosphate is altered by the non planar base-pair. These structural changes explain the observation that both the conformational change preceding phosphoryl transfer and phosphoryl transfer are reduced for GMP incorporation by $3D^{pol}$ (Arnold and Cameron, 2004b; Arnold et al., 2004) or AMP incorporation by the D238A derivative (Gohara et al., 2000, 2004). A purine:purine mispair likely disturbs the orientation of Asp-238 in the binding pocket, initiating a cascade of destabilizing events, movement of the 3′-OH, the β-phosphate and ultimately the entire triphosphate moiety of the incorrect nucleotide substrate. A pyrimidine:pyrimidine mispair likely increases the mobility of residues within the pocket, altering the orientation of Asp-238.

The orientation of the triphosphate moiety of the nucleotide substrate is fundamental for nucleotide incorporation not only for the RdRP but also for other polymerases (Beese et al., 1993; Cheetham and Steitz, 1999; Doublie et al., 1998; Johnson et al., 2003; Li et al., 1998; Yin and Steitz, 2002). Stabilization of the triphosphate conformation requires conserved structural motif A (Fig. 6). Stabilization of the triphosphate-metal complex in the active conformation requires of a network of hydrogen bonds provided mostly by the backbone of the residues in motif A (Fig. 6). Therefore, any movement of the motif A side chains located in the sugar-binding pocket will be transmitted through the rest of motif A, consequently perturbing the position of both the sugar and

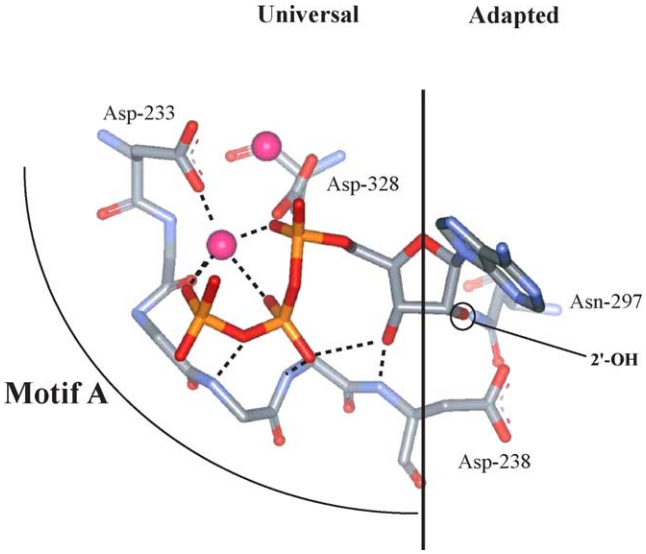

Fig. 6. A conserved mechanism for linking binding of a correct nucleotide to the efficiency of phosphoryl transfer. The nucleotide-binding pocket of all nucleic acid polymerases with a canonical "palm"-based active site is highly conserved. The site can be divided into two parts: a region that has "universal" interactions mediated by conserved structural motif A that organizes the metals and triphosphate for catalysis and a region that has "adapted" interactions mediated by conserved structural motif B that dictate whether ribo- or 2′-deoxribonucleotides will be utilized. In the classical polymerase, there is a motif A residue located in the sugar-binding pocket capable of interacting with motif B residue(s) involved in sugar selection. This motif A residue in other polymerases could represent the link between the nature of the bound nucleotide (correct vs. incorrect) to the efficiency of phosphoryl transfer as described herein for Asp-238 of $3D^{pol}$ (Gohara et al., 2004). Reproduced with permission from Biochemistry, 2004, submitted. © 1998 Am. Chem. Soc.

triphosphate and reducing the efficiency of phosphoryl transfer as described above for Asp-238 of $3D^{pol}$. The position of residues in motif A can be altered both by either the base or the ribose of the nucleotide (Fig. 6). Similar to Asn-297 (motif B) for $3D^{pol}$, T7 RNA polymerase uses His-784 (motif B) for hydrogen bonding to the 2′-OH of the NTP substrate (Brieba and Sousa, 2000). In HIV RT, Phe-160 (motif B) has van der Waals interactions with the 2′-H of the 2′-dNTP substrate (Gutierrez-Rivas et al., 1999). In the presence of a 2′-OH, Phe-160 will cause movement of Tyr-115 (motif A). Likewise, the presence of a motif B residue in DNA polymerases (e.g. T7, BF, KF, Taq and RB69) will cause movement of motif A via the motif A residue located in the sugar-binding pocket (Beese et al., 1993; Cheetham and Steitz, 1999; Doublie et al., 1998; Johnson et al., 2003; Li et al., 1998; Yin and Steitz, 2002).

Succinctly, the nucleotide-binding pocket of all polymerases can be divided into two parts: a universal portion and an adapted portion. Conserved structural motif A mediates the universal functions, whereas conserved structural motif B mediates the adapted function. These two motifs intersect in the sugar-binding pocket, providing a mechanism for inappropriate base pairing and/or sugar configuration to be identified and cause the appropriate reduction in phospho-

Table 3
Kinetic parameters for wild-type and G64S $3D^{pol}$-catalyzed nucleotide incorporation

Enzyme	Nucleotide	Kinetic parameters			Fidelity[a]
		$K_{d,app}$	k_{pol} (s^{-1})	k_{pol}/K_d ($\mu M^{-1}\ s^{-1}$)	
WT	ATP	134 ± 18	87 ± 4	0.65	–
	RTP	386 ± 42	0.011 ± 0.003	2.8×10^{-5}	2.3×10^4
	GTP	430 ± 98	0.014 ± 0.001	3.3×10^{-5}	2.0×10^4
G64S	ATP	161 ± 10	32 ± 2	0.20	–
	RTP	367 ± 43	0.0021 ± 0.0002	5.7×10^{-6}	3.5×10^4
	GTP	444 ± 66	0.0035 ± 0.0002	7.9×10^{-6}	2.5×10^4

[a] Fidelity is calculated as $[(k_{pol}/K_{d,app})_{ATP} + (k_{pol}/K_{d,app})_{incorrect}]/[(k_{pol}/K_{d,app})_{incorrect}]$ (Patel et al., 1991).

ryl transfer efficiency by moving the triphosphate moiety of the nucleotide substrate into a suboptimal orientation.

5. Amino acid residues at remote sites also contribute to RdRP fidelity

Recently, a poliovirus variant with decreased sensitivity to ribavirin was isolated (Pfeiffer and Kirkegaard, 2003). This poliovirus variant encodes a polymerase with a change of Gly-64 to Ser (G64S) mutation in the fingers subdomain (Pfeiffer and Kirkegaard, 2003). Analysis of the mutation frequency of the G64S virus by using a guanidine-resistance assay indicated that the G64S polymerase had an increase in incorporation fidelity.

The fidelity of the G64S $3D^{pol}$ has been evaluated by analyzing the incorporation of AMP, GMP and RMP (ribavirin) into sym/sub (Table 3) (Arnold and Cameron, 2004a). Nucleotide binding by G64S $3D^{pol}$ is equivalent to wild-type $3D^{pol}$ regardless of the nature of the nucleotide, correct or incorrect, consistent with the finding that binding is governed primarily by the triphosphate moiety (Table 3). However, the overall efficiency of RMP and GMP incorporation was reduced significantly relative to wild-type $3D^{pol}$, suggesting a decrease in either the conformational-change step or the phosphoryl-transfer step (Table 3). The fidelity of G64S $3D^{pol}$ increased compared to wild-type enzyme, and the capacity of the G64S substitution to permit decreased utilization of RTP could be explained by increased fidelity of this derivative relative to wild-type $3D^{pol}$. The mechanistic basis for this increased fidelity is a change in the stability of the activated ternary complex compared to wild-type $3D^{pol}$ (Arnold and Cameron, 2004a). The ability to show that an amino acid substitution in $3D^{pol}$ that increases polymerase fidelity causes a change in step 2 (Scheme 1) provides an undisputable link between this step and fidelity (Showalter and Tsai, 2002).

The structural basis for the increased fidelity observed for G64S $3D^{pol}$ is not currently known and may be difficult to discern, given the subtle difference in fidelity relative to wild-type and the lack of available RdRP co-crystal structures with RNA primer/template and nucleotide bound. The Gly-64 residue is located in the fingers domain (Fig. 7) of the polymerase, and it is not possible to suggest a direct mechanism for interaction with the nucleotide substrate given its remote location.

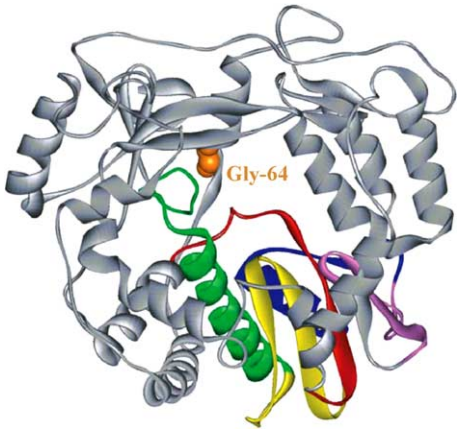

Fig. 7. Location of Gly-64 in the structural model of $3D^{pol}$. Model of $3D^{pol}$ (complete) based upon sequence and structural homology to rabbit hemorrhagic disease virus $3D^{pol}$ (Ng et al., 2002). The conserved structural motifs in the palm subdomain are colored as follows: motif A, red; motif B, green; motif C, yellow; motif D, blue; motif E, purple. van der Waal's projection of Gly-64 (orange). The image was rendered using the program WebLab Viewer Pro (Molecular Simulations Inc., San Diego, CA).

6. Implications of the kinetic, thermodynamic and structural basis for RdRP fidelity on the development of antivirals

The discovery that residues remote from the ribose-binding pocket can modulate fidelity is quite provocative. It is conceivable that small molecules can be developed that bind to surfaces of the polymerase and modulate fidelity. Compounds that increase incorporation fidelity should make the virus more susceptible to pressures that could be evaded by population diversity, for example, the immune system. Compounds that decrease incorporation fidelity should force the virus into error catastrophe. Clearly, this strategy will prevent the complications associated with nucleoside-based polymerase inhibitors. Importantly, these small molecules can be "recycled" in a mechanism in which the antiviral would bind

to the activated ternary complex, altering its fidelity and then be released.

Acknowledgement

We thank Ken Ng for the structural model of $3D^{pol}$ shown in Fig. 7.

References

Airaksinen, A., Pariente, N., Menendez-Arias, L., Domingo, E., 2003. Curing of foot-and-mouth disease virus from persistently infected cells by ribavirin involves enhanced mutagenesis. Virology 311, 339–349.

Arnold, J.J., Cameron, C.E., 2000. Poliovirus RNA-dependent RNA polymerase ($3D^{pol}$): assembly of stable, elongation-competent complexes by using a symmetrical primer-template substrate (sym/sub). J. Biol. Chem. 275, 5329–5336.

Arnold, J.J., Cameron, C.E., 2004a, unpublished observations.

Arnold, J.J., Cameron, C.E., 2004b. Poliovirus RNA-dependent RNA polymerase ($3D^{pol}$): pre-steady-state kinetic analysis of ribonucleotide incorporation in the presence of Mg^{2+}. Biochemistry 43, 5126–5137.

Arnold, J.J., Ghosh, S.K., Cameron, C.E., 1999. Poliovirus RNA-dependent RNA polymerase ($3D^{pol}$): divalent cation modulation of primer, template, and nucleotide selection. J. Biol. Chem. 274, 37060–37069.

Arnold, J.J., Gohara, D.W., Cameron, C.E., 2004. Poliovirus RNA-dependent RNA polymerase ($3D^{pol}$): pre-steady-state kinetic analysis of ribonucleotide incorporation in the presence of Mn^{2+}. Biochemistry 43, 5138–5148.

Beckman, R.A., Mildvan, A.S., Loeb, L.A., 1985. On the fidelity of DNA replication: manganese mutagenesis in vitro. Biochemistry 24, 5810–5817.

Beese, L.S., Friedman, J.M., Steitz, T.A., 1993. Crystal structures of the Klenow fragment of DNA polymerase I complexed with deoxynucleoside triphosphate and pyrophosphate. Biochemistry 32, 14095–14101.

Brieba, L.G., Sousa, R., 2000. Roles of histidine 784 and tyrosine 639 in ribose discrimination by T7 RNA polymerase. Biochemistry 39, 919–923.

Cheetham, G.M., Steitz, T.A., 1999. Structure of a transcribing T7 RNA polymerase initiation complex. Science 286, 2305–2309.

Crotty, S., Cameron, C.E., Andino, R., 2001. RNA virus error catastrophe: direct molecular test by using ribavirin. Proc. Natl. Acad. Sci. U.S.A. 98, 6895–6900.

Crotty, S., Maag, D., Arnold, J.J., Zhong, W., Lau, J.Y., Hong, Z., Andino, R., Cameron, C.E., 2000. The broad-spectrum antiviral ribonucleoside ribavirin is an RNA virus mutagen. Nat. Med. 6, 1375–1379.

De la Torre, J.C., Wimmer, E., Holland, J.J., 1990. Very high frequency of reversion to guanidine resistance in clonal pools of guanidine-dependent type 1 poliovirus. J. Virol. 2, 664–671.

Domingo, E., 1989. RNA virus evolution and the control of viral disease. Prog. Drug. Res. 33, 93–133.

Domingo, E., Escarmis, C., Sevilla, N., Moya, A., Elena, S.F., Quer, J., Novella, I.S., Holland, J.J., 1996. Basic concepts in RNA virus evolution. FASEB J. 10, 859–864.

Domingo, E., Martinez-Salas, E., Sobrino, F., de la Torre, J.C., Portela, A., Ortin, J., Lopez-Galindez, C., Perez-Brena, P., Villanueva, N., Najera, R., et al., 1985. The quasi-species (extremely heterogeneous) nature of viral RNA genome populations: biological relevance: a review. Gene 40, 1–8.

Doublie, S., Tabor, S., Long, A.M., Richardson, C.C., Ellenberger, T., 1998. Crystal structure of a bacteriophage T7 DNA replication complex at 2.2 Å resolution. Nature 391, 251–258.

Drake, J.W., 1993. Rates of spontaneous mutation among RNA viruses. Proc. Natl. Acad. Sci. U.S.A. 90, 4171–4175.

Drake, J.W., 1999. The distribution of rates of spontaneous mutation over viruses, prokaryotes, and eukaryotes. Ann. N.Y. Acad. Sci. 870, 100–107.

Drake, J.W., Holland, J.J., 1999. Mutation rates among RNA viruses. Proc. Natl. Acad. Sci. U.S.A. 96, 13910–13913.

Eggers, H.J., Tamm, I., 1965. Coxsackie A9 virus: mutation from drug dependence to drug independence. Science 148, 97–98.

Gohara, D.W., Arnold, J.J., Cameron, C.E., 2004. Poliovirus RNA-dependent RNA Polymerase ($3D^{pol}$): kinetic, thermodynamic and structural analysis of ribonucleotide selection. Biochemistry 43, 5149–5158.

Gohara, D.W., Crotty, S., Arnold, J.J., Yoder, J.D., Andino, R., Cameron, C.E., 2000. Poliovirus RNA-dependent RNA polymerase ($3D^{pol}$): structural, biochemical, and biological analysis of conserved structural motifs A and B. J. Biol. Chem. 275, 25523–25532.

Goodman, M.F., Keener, S., Guidotti, S., Branscomb, E.W., 1983. On the enzymatic basis for mutagenesis by manganese. J. Biol. Chem. 258, 3469–3475.

Gutierrez-Rivas, M., Ibanez, A., Martinez, M.A., Domingo, E., Menendez-Arias, L., 1999. Mutational analysis of Phe160 within the "palm" subdomain of human immunodeficiency virus type 1 reverse transcriptase. J. Mol. Biol. 290, 615–625.

Hansen, J.L., Long, A.M., Schultz, S.C., 1997. Structure of the RNA-dependent RNA polymerase of poliovirus. Structure 5, 1109–1122.

Holland, J., Spindler, K., Horodyski, F., Grabau, E., Nichol, S., VandePol, S., 1982. Rapid evolution of RNA genomes. Science 215, 1577–1585.

Holland, J.J., Domingo, E., de la Torre, J.C., Steinhauer, D.A., 1990. Mutation frequencies at defined single codon sites in vesicular stomatitis virus and poliovirus can be increased only slightly by chemical mutagenesis. J. Virol. 64, 3960–3962.

Huang, Y., Beaudry, A., McSwiggen, J., Sousa, R., 1997. Determinants of ribose specificity in RNA polymerization: effects of Mn^{2+} and deoxynucleoside monophosphate incorporation into transcripts. Biochemistry 36, 13718–13728.

Irurzun, A., Perez, L., Carrasco, L., 1992. Involvement of membrane traffic in the replication of poliovirus genomes: effects of brefeldin A. Virology 270, 251–253.

Johnson, S.J., Taylor, J.S., Beese, L.S., 2003. Processive DNA synthesis observed in a polymerase crystal suggests a mechanism for the prevention of frameshift mutations. Proc. Natl. Acad. Sci. U.S.A. 100, 3900–3985.

Kearney, C.M., Thomson, M.J., Roland, K.E., 1999. Genome evolution of tobacco mosaic virus populations during long-term passaging in a diverse range of hosts. Arch. Virol. 144, 1513–1526.

Koonin, E.V., 1991. The phylogeny of RNA-dependent RNA polymerases of positive-strand RNA viruses. J. Gen. Virol. 72, 2197–2206.

Lee, C.H., Gilbertson, D.L., Novella, I.S., Huerta, R., Domingo, E., Holland, J.J., 1997. Negative effects of chemical mutagenesis on the adaptive behavior of vesicular stomatitis virus. J. Virol. 71, 3636–3640.

Li, Y., Korolev, S., Waksman, G., 1998. Crystal structures of open and closed forms of binary and ternary complexes of the large fragment of *Thermus aquaticus* DNA polymerase I: structural basis for nucleotide incorporation. EMBO J. 17, 7514–7525.

Liu, J., Tsai, M.-D., 2001. DNA polymerase beta: pre-steady-state kinetic analyses of dATP alpha S stereoselectivity and alteration of the stereo selectivity by various metal ions and by site-directed mutagenesis. Biochemistry 40, 9014–9022.

Ng, K.K., Cherney, M.M., Vazquez, A.L., Machin, A., Alonso, J.M., Parra, F., James, M.N., 2002. Crystal structures of active and inactive conformations of a caliciviral RNA-dependent RNA polymerase. J. Biol. Chem. 277, 1381–1387.

Parvin, J.D., Moscona, A., Pan, W.T., Leider, J.M., Palese, P., 1986. Measurement of the mutation rates of animal viruses: influenza A virus and poliovirus type 1. J. Virol. 59, 377–383.

Patel, S.S., Wong, I., Johnson, K.A., 1991. Pre-steady-state kinetic analysis of processive DNA replication including complete characterization of an exonuclease-deficient mutant. Biochemistry 30, 511–525.

Pfeiffer, J.K., Kirkegaard, K., 2003. A single mutation in poliovirus RNA-dependent RNA polymerase confers resistance to nucleoside analogs via increased fidelity. Proc. Natl. Acad. Sci. U.S.A. 100, 7289–7294.

Pincus, S.E., Diamond, D.C., Emini, E.A., Wimmer, E., 1986. Guanidine-selected mutants of poliovirus: mapping of point mutations to polypeptide 2C. J. Virol. 57, 638–646.

Ruiz-Jarabo, C.M., Ly, C., Domingo, E., de la Torre, J.C., 2003. Lethal mutagenesis of the prototypic arenavirus lymphocytic choriomeningitis virus (LCMV). Virology 308, 37–47.

Sanchez, G., Bosch, A., Gomez-Mariano, G., Domingo, E., Pinto, R.M., 2003. Evidence for quasi-species distributions in the human hepatitis A virus genome. Virology 315, 34–42.

Severson, W.E., Schmaljohn, C.S., Javadian, A., Jonsson, C.B., 2003. Ribavirin causes error catastrophe during Hantaan virus replication. J. Virol. 77, 481–488.

Showalter, A.K., Tsai, M.D., 2002. A reexamination of the nucleotide incorporation fidelity of DNA polymerases. Biochemistry 41, 10571–10576.

Steinhauer, D.A., de la Torre, J.C., Meier, E., Holland, J.J., 1989. Extreme heterogeneity in populations of vesicular stomatitis virus. J. Virol. 63, 2072–2080.

Tabor, S., Richardson, C.C., 1989. Effect of manganese ions on the incorporation of dideoxynucleotides by bacteriophage T7 DNA polymerase and *Escherichia coli* DNA polymerase I. Proc. Natl. Acad. Sci. U.S.A. 86, 4076–4080.

Ward, C.D., Stokes, M.A., Flanegan, J.B., 1988. Direct measurement of the poliovirus RNA polymerase error frequency in vitro. J. Virol. 62, 558–562.

Yin, Y.W., Steitz, T.A., 2002. Structural basis for the transition from initiation to elongation transcription in T7 RNA polymerase. Science 298, 1387–1395, Epub September 19, 2002.

Young, K.C., Lindsay, K.L., Lee, K.J., Liu, W.C., He, J.W., Milstein, S.L., Lai, M.M., 2003. Identification of a ribavirin-resistant NS5B mutation of hepatitis C virus during ribavirin monotherapy. Hepatology 38, 869–878.